Quantum tricritical point in the temperature-pressure-magnetic field phase diagram of CeTiGe_{3}

Udhara S. Kaluarachchi, Valentin Taufour, Sergey L. Bud'ko, and Paul C. Canfield

Phys. Rev. B **97**, 045139 — Published 22 January 2018

DOI: 10.1103/PhysRevB.97.045139

Quantum tricritical point in the temperature-pressure-magnetic field phase diagram of $CeTiGe_3$

Udhara S. Kaluarachchi,[1,2] Valentin Taufour*,[1] Sergey L. Bud'ko,[1,2] and Paul C. Canfield[1,2]

[1] *The Ames Laboratory, US Department of Energy, Iowa State University, Ames, Iowa 50011, USA*
[2] *Department of Physics and Astronomy, Iowa State University, Ames, Iowa 50011, U.S.A.*

We report the temperature-pressure-magnetic field phase diagram of the ferromagnetic Kondo-lattice $CeTiGe_3$ determined by means of electrical resistivity measurements. Measurements up to ~ 5.8 GPa reveal a rich phase diagram with multiple phase transitions. At ambient pressure, $CeTiGe_3$ orders ferromagnetically at $T_C = 14$ K. Application of pressure suppresses T_C, but a pressure induced ferromagnetic quantum criticality is avoided by the appearance of two new successive transitions for $p > 4.1$ GPa that are probably antiferromagnetic in nature. These two transitions are suppressed under pressure, with the lower temperature phase being fully suppressed above 5.3 GPa. The critical pressures for the presumed quantum phase transitions are $p_1 \cong 4.1$ GPa and $p_2 \cong 5.3$ GPa. Above 4.1 GPa, application of magnetic field shows a tricritical point evolving into a wing structure phase with a quantum tricritical point at 2.8 T at 5.4 GPa, where the first order antiferromagnetic-ferromagnetic transition changes into the second order antiferromagnetic-ferromagnetic transition.

INTRODUCTION

Quantum phase transitions (QPT) in metallic ferromagnets have been studied for many years and remain a subject of great current interest [1]. The paramagnetic (PM) to ferromagnetic (FM) transition can be suppressed with nonthermal control parameters such as pressure, chemical composition or external field often leading to a $T = 0$ K, QPT. However, according to the current theoretical models, when suppressing the FM phase with a clean parameter such as pressure, a continuous PM to FM transition is not possible. Instead, the transition becomes of the first order or a modulated magnetic phase can appear. The possibility of a first-order transition or the appearance of modulated magnetic phases was first discussed in Refs. 2 and 3. In the case of the transition becoming of the first order, a wing structure was predicted in Ref. 4 and observed in UGe_2 [5] and $ZrZn_2$ [6]. The case of the appearance of a modulated magnetic phase is more complex[2, 3, 7–12] and an experimental examples were found in $LaCrGe_3$ [12] and CeRuPO [13]. Observation of both tricritical wings and modulated magnetic phase in $LaCrGe_3$ is a good example of a complex phase diagram and provides a new example of the richness of the phase diagram of metallic quantum ferromagnets [14]. Recently, Belitz and Kirkpatrick proposed that such complex phase diagram is due to quantum fluctuation effects [15].

Cerium based compounds have attracted attention due to interesting ground states, such as heavy-fermion, unconventional superconductor [16, 17], Kondo insulator [18], magnetic ordering [19, 20], etc. Whereas many Ce-based compounds manifest an antiferromagnetic (AFM) ground state, only few systems are known with FM order and pronounced Kondo effects. CeRuPO [13], $CeAgSb_2$ [21, 22], $CeNiSb_3$ [23], $CePd_2Ge_3$ [24] and $Ce_2Ni_5C_3$ [25] are some examples of the Ce-based ferromagnets, which show complex phase diagrams under the application of pressure. Interestingly, the FM transition in these materials is suppressed with the pressure and new magnetic (most probably AFM) phases appear before the Curie temperature reaches 0 K but no wing structure in the T-H-p phase diagrams has been observed so far. According to the recent theoretical work by Belitz *et al.* [15], it is possible to have unobservable tricritical wings inside the AFM dome. In most of these cases, lack of in-field measurements under pressure prevents from constructing the temperature-pressure-field phase diagram and getting a better understanding of the system. Therefore, it is interesting to further investigate the temperature-pressure-field effect on a Ce-based ferromagnetic system. To address this, we present measurements of electrical resistivity under pressure up to ~ 5.8 GPa and magnetic field up to 9 T on ferromagnetic $CeTiGe_3$.

$CeTiGe_3$ is one of the relatively rare examples of a ferromagnetic Kondo lattice (γ=75 mJ mol^{-1} K^{-2} [26]); it orders with a Curie temperature, $T_C = 14$ K [27]. It crystallizes in the hexagonal perovskite $BaNiO_3$ - type structure ($P6_3/mmc$) [27]. Magnetization measurements show highly anisotropic behavior with c-axis being the easy axis of magnetization [26]. A Curie-Weiss fit to the susceptibility data yields an effective moment of 2.5 μ_B, consistent with the reported values [26] and nearly equal to the value for free-ions trivalent Ce (2.54 μ_B). The reported saturation moment at 2 K from the magnetization data (1.72 μ_B/Ce) along the c-axis [26] is comparable with the value obtained from the neutron diffraction study(1.5 μ_B/Ce) [28]. Substitution of titanium by vanadium ($CeTi_{1-x}V_xGe_3$) causes a suppression of the Curie temperature down to 3 K at $x = 0.3$ and suggests a possible quantum critical point or phase transition near $x \approx 0.35$ [28]. In contrast to the effect of substitution, a very small, initial positive pressure derivative of T_C ($dT_C/dp \approx 0.3$ K GPa^{-1} up to 1 GPa) suggests that $CeTiGe_3$ is located near the maximum of the magnetic

ordering temperature in the Doniach model [28]. However, all substitution and pressure measurements have been done on the polycrystalline material and only to modest pressure, $p < 1$ GPa. To get a better understanding of T-p-H phase diagram, possible FM instability and QCP it is important to perform high pressure studies on single crystalline samples of $CeTiGe_3$ over a wide pressure range.

EXPERIMENTAL METHODS

Single crystals of $CeTiGe_3$ were grown using a high temperature solution growth technique [29, 30]. A mixture of elemental Ce, Ti and Ge was placed in a 2 mL fritted alumina crucible [31] with a molar ratio of Ce:Ti:Ge = 4:1:19 [26] and sealed in a silica ampule under a partial pressure of high purity argon gas. The sealed ampule was heated to 1200 °C over 10 hours and held there for 5 hours. It was cooled to 900°C over 120 hours and excess liquid was decanted using a centrifuge. A good quality sample (based on the residual resistivity ratio) for the pressure study was selected after ambient pressure characterization by the magnetization and resistivity measurements. Temperature and field dependent resistance measurements were carried out using a Quantum Design (QD) Physical Property Measurement System (PPMS) from 1.8 K to 300 K. The *ac*-resistivity ($f = 17$ Hz) was measured by the standard four-probe method with the 1 mA current in the *ab* plane. Four Au wires with diameters of 12.5 μm were spot welded to the sample. A magnetic field, up to 9 T, was applied along the *c*-axis, which corresponds to the magnetization easy axis [26]. A modified Bridgman cell [32] was used to generate pressure for the resistivity measurement. A 1:1 mixture of *n*-pentane:iso-pentane was used as a pressure medium. The solidification of this medium occurs around ~6-7 GPa at room temperature [33–37]. The pressure at low temperature was determined by the superconducting transition temperature of Pb [38].

RESULTS AND DISCUSSION

The temperature dependencies of the in-plane resistivity of single crystalline $CeTiGe_3$ under various pressures up to 5.76 GPa are shown in Fig. 1 (a). At ambient pressure, the resistivity exhibits typical Kondo-lattice behavior with a broad minimum ~ 190 K followed by a maximum at $T_{max} = 31$ K. The T_{max} is assumed to be related to the Kondo interaction with a changing population of crystal electric field levels [26, 39–41]. The FM transition manifests itself in the resistivity data as a sharp drop at $T_C = 14.2$ K. Similar values of T_C have been reported from polycrystalline and single crystalline samples [26–28]. The residual resistivity ratio (RRR) is 19, a value

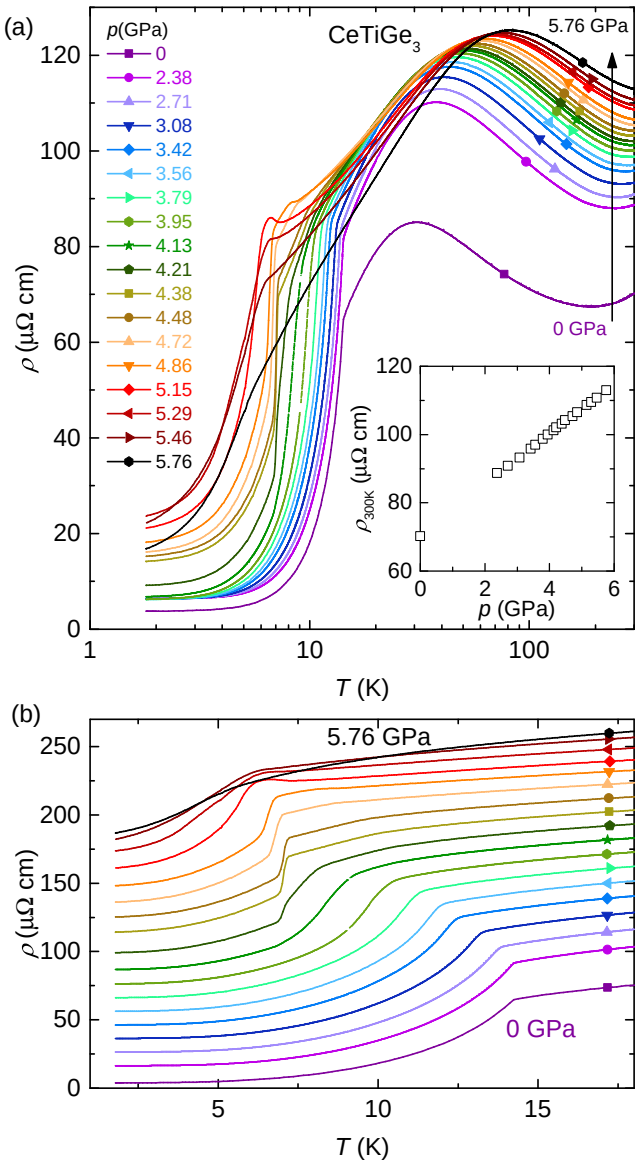

FIG. 1. (Color online) (a) Temperature dependence of the in-plane resistivity, $\rho(T)$, of a $CeTiGe_3$ single crystal under various pressures, p, up to 5.76 GPa on a semi-log plot. The resistivity at 300 K linearly increase with the pressure at a rate of 7.4 $\mu\Omega$ cm GPa^{-1} from 0 to 5.76 GPa as shown in the inset. (b) Low temperature resistivity at various pressures. Data are offset by increments of 10 $\mu\Omega$ cm for clarity.

that suggests a rather good quality of the sample. Upon application of pressure the resistivity at room temperature increases linearly with a rate of 7.4 $\mu\Omega$ cm GPa^{-1} over the whole pressure range (see inset of Fig. 1 (a)), both the local maximum and local minimum in the resistivity broaden and move to higher temperatures with increasing pressure. The evolution of the low temperature resistivity is shown in Fig. 1 (b); data are offset by increments of 10 $\mu\Omega$ cm for clarity.

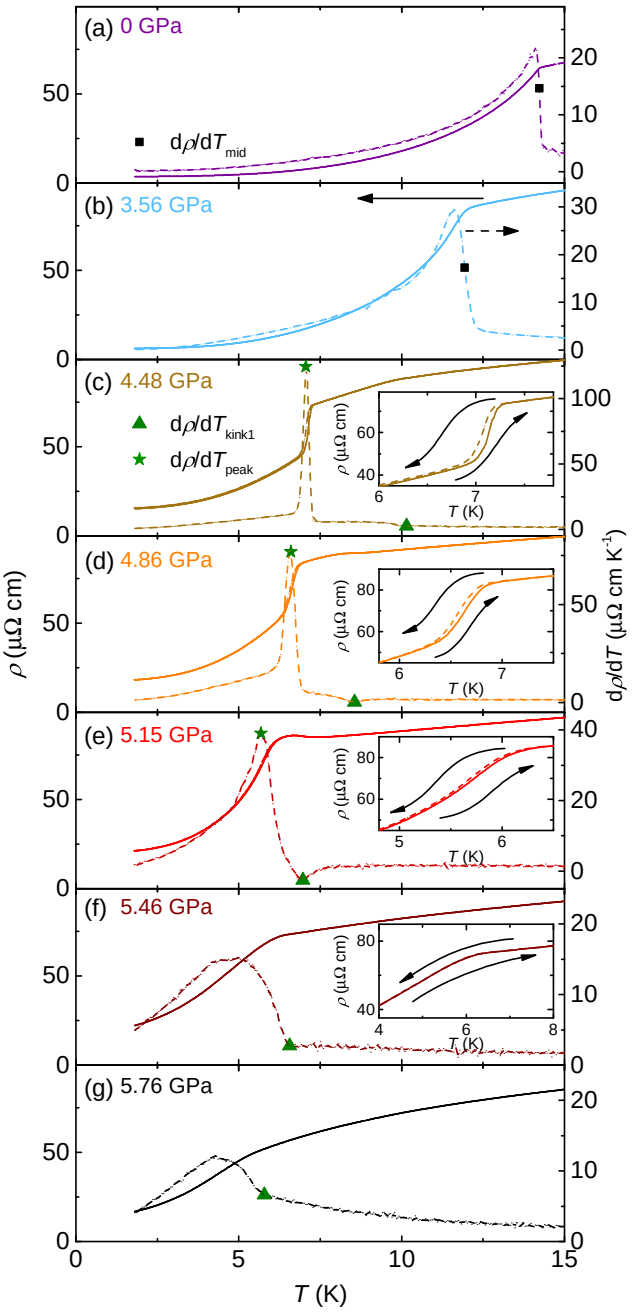

FIG. 2. (Color online) Low temperature, in-plane resistivity (left axis) and its corresponding temperature derivative (right axis) of $CeTiGe_3$ for several representative pressure regions (a)-(b) $p < 4.1$ GPa, (c)-(e) 4.1 GPa $< p <$ 5.3 GPa and (f)-(g) 5.3 GPa $< p$. The solid symbols mark the characteristic temperatures that are associated with phase transitions: black square-PM to FM, green triangle- PM to MP1/MP1' and green star- MP1 to MP2. The insets of (c)-(e) show the observed hysteretic behavior at their representative pressures. However, no hysteretic behavior is observed above 5.3 GPa as shown in inset of (f).

Figure 2 shows the evolution of the low temperature resistivity and its temperature derivatives in three selected pressure regions; (I) $p < 4.1$ GPa (II) 4.1 GPa $< p <$ 5.3 GPa and (III) $p >$ 5.3 GPa. Below 4.1 GPa the FM transition is seen as a sharp change of slope in the resistivity and transition temperature is obtained from the sharpest increase of $d\rho/dT$ (black square) (Figs. 2 (a)-(b)). The FM transition temperature initially shows a weak increase with pressure and then decreases with further applied pressure up to 4.1 GPa. Between 4.1-5.3 GPa, the onset of magnetic transition 1 (MP1) and magnetic transition 2 (MP2) are revealed as a kink/upturn and a sharp drop in the $\rho(T)$ as shown in Figs. 2 (c)-(e). From the transport measurements we can not unambiguously identify MP1, MP2, (and MP1', MP3, MP4) as the magnetic phases. However, observation of the metamagnetic transitions under application of field (see Fig. 5(c)) strongly suggests that, these are probably magnetic phases. The features in the resistivity can be clearly seen in the temperature derivative of the resistivity (right axis of Fig. 2). Transition temperatures of PM-MP1 and MP1-MP2 are obtained from the kink/minimum (green up-triangle, Figs. 2 (c)-(e)) and sharp peak (green star) in $d\rho/dT$ (Figs. 2 (c)-(e)) respectively. Although the magnetic ordering wave vector of MP1 is unknown, the feature in the resistivity is similar to that associated with superzone gap formation [42] and suggests an AFM nature for MP1. Both MP1 and MP2 transitions are observed between 4.1 to 5.3 GPa and thermal hysteresis in ρ for MP2 up to 5.3 GPa (inset of Figs. 2 (c)-(e)) indicates a first-order nature for this transition. On further increase of pressure, above 5.3 GPa, MP2 disappears and a new magnetic transition, MP1', continue to decrease with the increase of pressure and no thermal hysteresis is observed (Figs. 2 (f)-(g)). Although features in the ρ(T) corresponding to the MP1 and MP1' transitions look similar, it is unclear whether it is same phase or not. Figure 3 shows the evolution of the temperature derivative of the resistivity for representative pressures. Solid symbols represent the criteria described in Fig. 2.

The temperature-pressure ($T - p$) phase diagram of $CeTiGe_3$ obtained from the resistivity measurements, is summarized in Fig. 4 (a). At low pressures, the Curie temperature of the ambient pressure, FM phase (solid squares) shows a very weak pressure dependence and then decreases with pressure. For 4.1 GPa $\leq p \leq$ 5.3 GPa, there is an evidence for two phase transitions, MP1 and MP2 in the $\rho(p, T)$ curves, which interrupted the initial FM phase transition line. The merging of the PM-FM, PM-MP1 and FM-MP1 transition lines is called the Lifshitz point [43]. The second order PM-FM transition becomes of the first order at a tricritical point (TCP) (see text below) as shown by the horizontal arrow. A similarly complex $T - p$ phase diagram has been observed in $CeNiSb_3$ [23] and the recently studied itinerant ferromagnet $LaCrGe_3$ [12]. Pressure induced transitions from

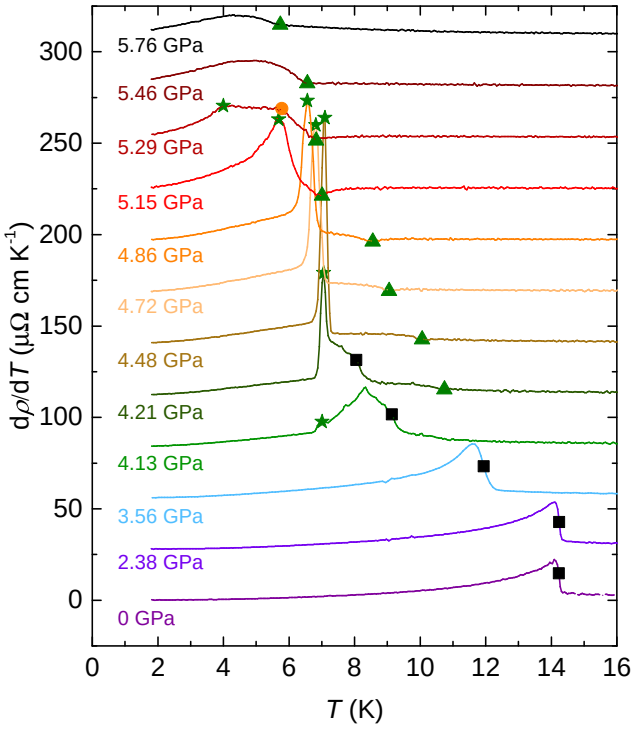

FIG. 3. (Color online) Evolution of the temperature derivative of the resistivity at low temperature for representative pressures. The data are vertically offset by 28 $\mu\Omega\,\mathrm{cm\,K^{-1}}$ to reduce overlap. Solid symbols represent the criteria described in Fig.2. At 5.29 GPa there is an additional anomaly in the $\mathrm{d}\rho/\mathrm{d}T$ as shown by the orange circle.

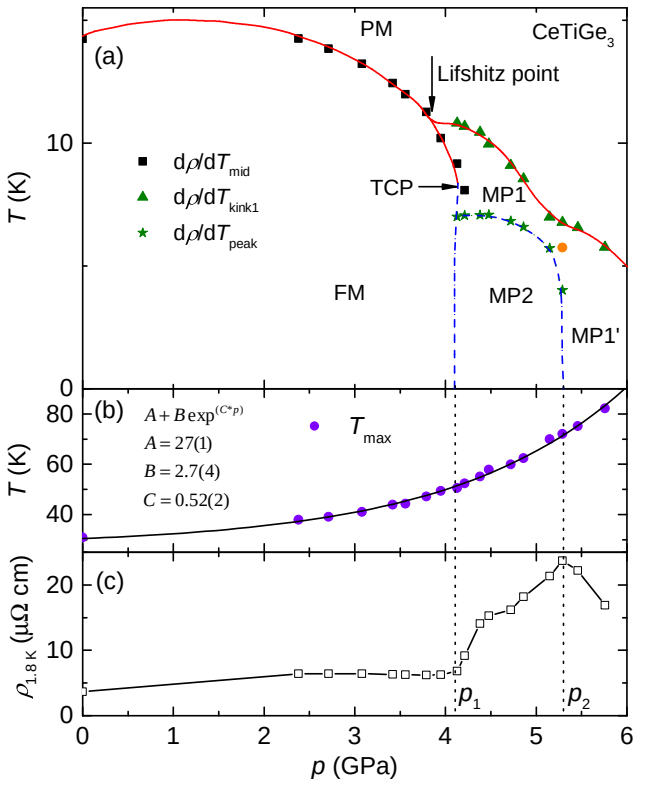

FIG. 4. (Color online)(a) $T-p$ phase diagram of $CeTiGe_3$ in zero applied field. Transition temperatures are determined from the anomalies in $\mathrm{d}\rho/\mathrm{d}T$ as shown in Fig. 2 and Fig. 3 . The values of critical pressure p_1 and p_2 are 4.1 and 5.3 GPa respectively. Solid lines are guide to the eye and dashed lines are suggested extrapolations of phase boundaries. The red and blue color line represent the second and first order phase transitions. The vertical and horizontal arrows represent the Lifshitz and tricritical point respectively. (b) Maximum in resistivity, T_{max} (shown in Fig. 1(a)), as a function of pressure increase as a exponential function. (c) Pressure dependence of the ρ at 1.8 K.

FM to AFM state are also observed in several other Ce-based compounds, such as $CeAgSb_2$ [22], $CeNiSb_3$ [23], $CePd_2Ge_3$ [24], $Ce_2Ni_5C_3$ [25] and CeRuPO [13]. Above 5.3 GPa, the low temperature MP2 phase disappears and MP1' continue to decrease with the increase of pressure. As mentioned above, it is unclear whether there is a phase boundary between MP1 and MP1' near 5.3 GPa.

In addition to the $T-p$ phase diagram, we find that, T_{max} exponentially increases from 31 K to 82 K upon increasing pressure (Fig. 4 (b)). The smooth change of T_{max} indicates that the existence of the new phases is not associated with a discontinuous changes in the electronic or crystal structure or CEF splitting. Figure 4 (c) shows the pressure evolution of the resistivity at 1.8 K. The results show breaks in $\rho_{1.8K}(p)$ at p_1 (FM to MP2) and a maximum at p_2 (MP2 to MP1). The exact nature of the phase transitions at p_1 and p_2 are not known and to resolve this, it would be useful to study the magnetic ordering wave vector under pressure.

Application of an external magnetic field adds another dimension to our phase diagram and different behavior of the resistivity anomalies under magnetic field allow us to explore further new phase regions of this material. Figure 5 (a) shows the temperature dependence of ρ at different magnetic fields, applied along the c-axis, at 4.48 GPa. The sharp drop in the resistivity at low fields ($\mu_0 H \leq 0.3$ T) broadens at higher fields. These data manifest hysteretic behavior up to 0.5 T, indicating the first order nature of the transition. The zero-field kink in the resistivity, at 9.8 K, changes into a hump with the increase of field (0.25 T) and disappears at 0.3 T. Another hump like feature appears above 0.35 T and broadens with further increase of the field. These features can be clearly observed in temperature derivative shown in Fig. 5 (b).

The field dependence of $\rho\,(p = 4.48\,\mathrm{GPa})$ below 7 K shows a metamagnetic transition with a low field plateau followed by a step-like feature and develops into two transitions above 7 K (Fig. 5 (c)). The solid and dashed lines represent the field increasing ($\rho_{\mathrm{up}}(H)$) and decreasing ($\rho_{\mathrm{down}}(H)$) respectively. The difference be-

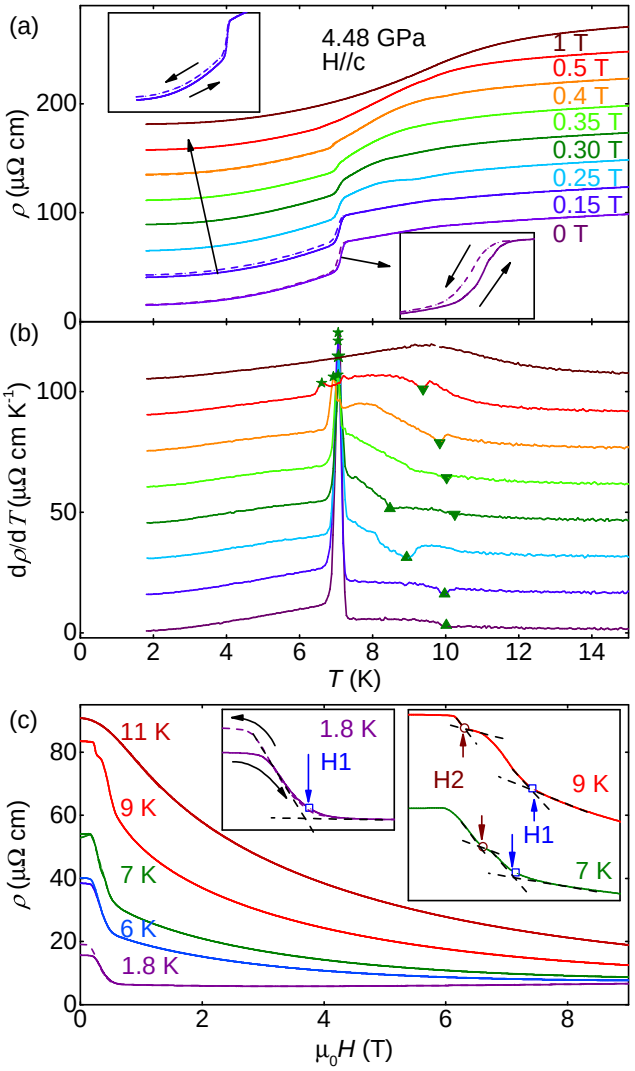

FIG. 5. (Color online)(a) Temperature dependence of the resistivity at various fixed fields for $p = 4.48$ GPa and $H \,||\, c$. The data are vertically shifted by integer of 25 $\mu\Omega$ cm to avoid overlapping. The insets show the observed hysteretic behavior in temperature scan. Continuous and dashed lines represent the temperature increasing and decreasing respectively. (b) Corresponding temperature derivative ($d\rho/dT$) of (a). The data are vertically shifted by integer of 15 $\mu\Omega$ cm K^{-1} to avoid overlapping. Solid symbols represent the criteria use to obtain the teansition temperatures at various magnetic fields. (c) Field dependence of the resistivity at fixed temperatures. For these data the sample was cooled in zero field and then $\rho(H)$ data was collected for increasing field ($\rho_{\rm up}$) and then decreasing field ($\rho_{\rm down}$). Then increase the temperature to the desired value and data was collected for increasing and decreasing field. Continuous and dashed lines represent the field increasing and decreasing respectively. Insets show the observed hysteretic behavior and the criteria used to obtain the transition fields. Above 7 K no hysteretic behavior is observed.

tween $\rho_{\rm up}(H)$-$\rho_{\rm down}(H)$ shows a sizable deviation (ρ is smaller in the increasing-field than the decreasing-field) for $0 \leq H \leq 0.3$ T range. In Fig. 5, hysteresis is apparent not only in the transition temperature (Fig. 5 (a)) and transition field (Fig. 5 (c)), but also in the magnitude of the resistivity. Similar hysteretic behavior is observed in the $CeAuSb_2$ [44–46] and $CeTAl_4Si_2$ (T = Rh, Ir) [47]. Based on the hysteretic behavior, we can conclude these metamagnetic transitions are likely associated with a first-order phase transition. The observed hysteresis in the magnitude of resistivity indicates the possibility of magnetic domains. At temperatures above 11 K, the resistivity shows a very broad anomaly and no transition has been observed. Criteria used to obtain transition fields are shown in the inset of Fig. 5 (c).

Figures 6 (a)-(d) show the $T - H$ phase diagrams at representative pressures. Transition temperatures determined by T-sweep measurements are shown by closed symbols and anomalies appeared in isothermal H-sweep measurements are shown by open symbols. Continuous blue and red lines indicate the first order and second order transitions respectively (based on the presence or lack of hysteretic behavior respectively). The red circle represents the TCP determined by Fig. 6 (e). Temperature dependence hysteresis widths for the transition at H1 are shown in Fig. 6 (e). The data are vertically offset by 0.03 T to avoid overlap. Clear hysteresis at low temperature gradually decreases with increasing temperature and disappears at a TCP as shown by a vertical arrow. In contrast to the wing-critical-point (WCP) in UGe_2 [5] and $LaCrGe_3$ [14], here we observed a TCP in the $T - H$ phase diagram where first order transition changes into the second order transition. This TCP corresponds to the boundary of the wing structure similar to UGe_2 [5] and $LaCrGe_3$ [14]. The $T - H$ phase diagrams of $CeTiGe_3$ for pressures between 4.1 - 5.3 GPa show complex behavior. Three magnetic phases (MP1, MP1' and MP2) are identified by the anomalies in the resistivity measurement. Both MP1 and MP1' phases are separated by MP2 phase by a first order transition as shown in Figs. 6 (a)-(c). For pressures between 4.1-5.3 GPa, these $T - H$ phase diagrams are similar to those found for $CeRu_2Al_2B$ [48], which undergoes a second order AFM transition that is followed by a first order FM transition as a function of temperature. Above 5.3 GPa, only two magnetic phases; MP1' and MP4 are identified by the resistivity measurements and there is no longer a first order phase transition boundary observed.

Figure 7 shows the constructed $T - H$ phase diagrams for pressures between 4.21 to 5.76 GPa. There is a clear difference in the $T - H$ phase diagrams below 4.86 GPa and above 5.46 GPa. $T - H$ phase diagram for the intermediate pressure, 5.29 GPa, shows a complex behavior. Also, we observed an additional shoulder-like anomaly in $\rho(H)$ at 5.76 GPa (gray color star in Fig. 8 (c) and Fig. 7). When the temperature was increased, it became broadened and merged with H1 and no loner resolvable. H1,

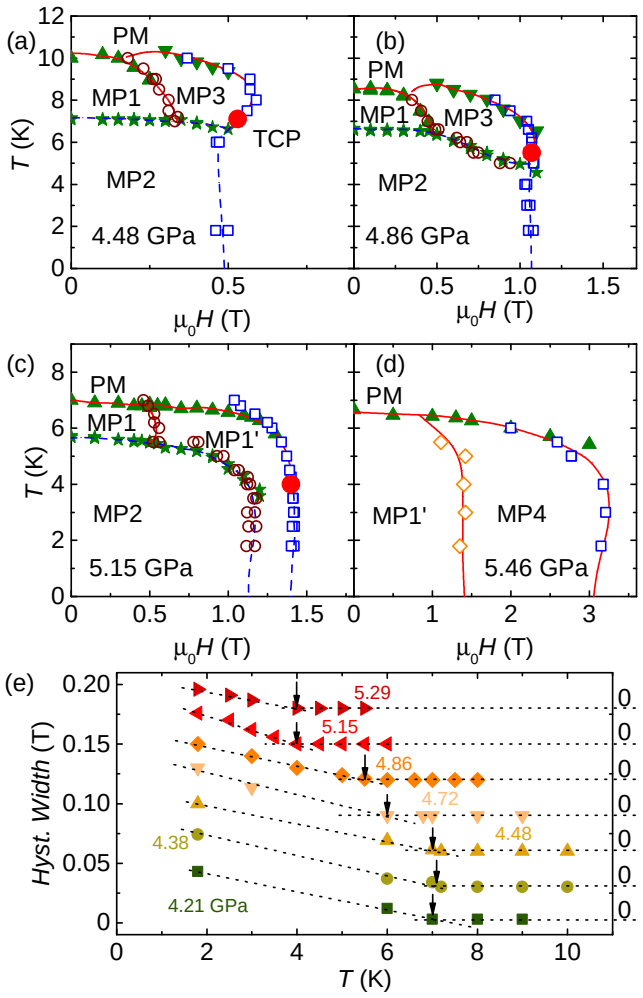

FIG. 6. (Color online) $T-H$ phase diagrams for various pressures: (a) 4.48 GPa (b) 4.86 GPa (c) 5.15 GPa and (d) 5.46 GPa, determine by tracking various anomalies in temperature and field derivatives of resistivity measurement as shown by Fig. 5. Solid and open symbols represent transition temperatures determined by T-sweeps and transition fields determined by H-sweeps (as described in Fig. 5) respectively. Continuous blue and red lines indicate the first order and second order transitions respectively. (e) Temperature dependence of hysteresis widths for the transition at H1 at various pressures. The data are vertically offset by 0.03 T to avoid overlap. Vertical arrows represent the estimated tricritical points for each pressure. Zero for each data set shown on right-hand axis.

H2 and H3 are the anomalies observed in $\rho(H)$ data as shown in Fig. 5 (c) and Figs. 8 (b)-(c)

Figure 8 (a) shows the field dependence of the resistivity at 1.8 K, $\rho(H)$, for different pressures. For the pressures in between p_1 and p_2, $\rho(H)$ for an increasing magnetic field shows a clear metamagnetic transition with a substantial ($>40\%$), drop of resistivity. For higher pressures, the sharp drop in the $\rho(H)$ disappears and several metamagnetic transitions can be observed. Figures 8 (b) and (c) show the representative magnetoresistance data for $4.1\,\text{GPa} < p < 5.3\,\text{GPa}$ and $p > 5.3\,\text{GPa}$ respectively. Transition fields determined by H-sweeps measurements are shown by the open symbols. To estimate the transition width, we used the field derivative of the resistivity at 1.8 K, as shown in Figs. 8(d) and (e). The minimum at H1 is fitted with Gaussian+linear-background and obtained the width of the Gaussian distribution. The blue color lines in Figs. 8(b) and (c) represent the fitted curves to the data. We noticed that the transition width (Fig. 8 (f) right axis) at H1 at 1.8 K remains small for the first-order transition and becomes broad in the second-order regime. Using linear extrapolation as represented by red dashed lines, we obtained pressure corresponding to the TCP at 1.8 K, which is 5.3 GPa. In addition to that, the temperature dependence hysteresis width for transition H1 at 1.8 K is also suppressed with the pressure and disappeared above 5.3 GPa as shown in Fig. 8 (f) left axis. Figure 8 (g) shows the $H-p$ phase diagram at 1.8 K constructed from the above criteria. The magnetic field that corresponds to the H1 transition is shifted up with pressure. Its extrapolation down to zero yields $p \cong 4.1$ GPa, which is in agreement with the p_1 obtained from T-p diagram (Fig. 4 (a)). We observe the increasing rate of metamagnetic transition field with respect to pressure, changes near 5.3 GPa.

Similar $H-p$ phase diagrams at low temperature have been observed in $LaCrGe_3$ [14] and $CeRu_2(Si_{1-x}Ge_x)_2$ [49, 50] system. $CeRu_2Ge_2$ is a local moment system [51], while $CeRu_2Si_2$ is itinerant [52]. Application of pressure to $CeRu_2Ge_2$ gives nearly same magnetic phase diagram as that of $CeRu_2(Si_{1-x}Ge_x)_2$ [53, 54]. Observed transport and de Haas-van Alphen data suggest that, for this system, change of the f-electron nature from local to itinerant occurs when the FM phase disappears [49]. On the other hand, itinerant ferromagnet $LaCrGe_3$ show tricritical wings as well as modulated magnetic phase. Interestingly, $T-p-H$ phase diagram of both $LaCrGe_3$ [14] and $CeRu_2Ge_2$ [50] without AFM states is similar to the itinerant weak ferromagnet like UGe_2 [5]. This similarity might imply that the physics behind these phase diagrams are not very different. In UCoAl [55] an additional anomaly is observed at the end of the tricritical wings similar to what we observe in $CeTiGe_3$. It is possible that the quantum wing critical point in UCoAl is in fact a quantum tricritical point similar to $CeTiGe_3$. However, the situation is not as clear, since, unlike $CeTiGe_3$, the new anomaly is not observed as a phase boundary in the low pressure region (i.e. there is no observed Lifshitz point in UCoAl). In addition, the position of the quantum wing critical point in UCoAl is unclear and was proposed to be located at higher pressures [56]. In light of the double wing structure observed in $LaCrGe_3$ [14], UGe_2 [57] and $ZrZn_2$ [58, 59], it is also possible that the additional anomaly corresponds to a

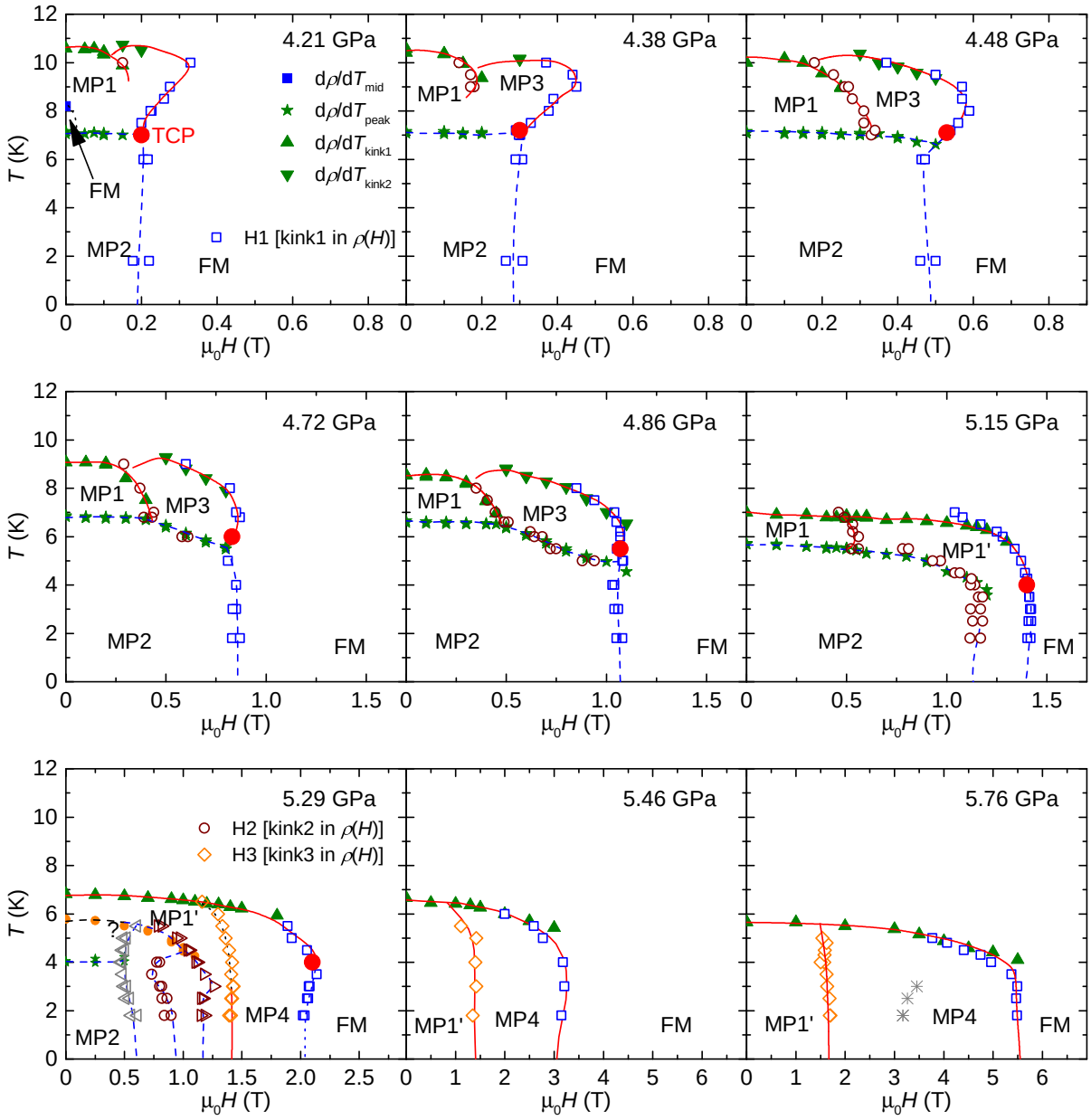

FIG. 7. (Color online) $T-H$ phase diagrams, including those shown in Fig. 6 (a)-(d,) at various increasing applied pressures. At 5.29 GPa, $T-H$ phase diagrams show a complex behavior and with additional metamagnetic transitions (gray and brown open triangles) in $\rho(H)$ data (raw data are not shown). H1, H2 and H3 are the anomalies observed in $\rho(H)$ data as shown in Fig. 5 (c) and Figs. 8 (b)-(c).

second wing.

The projection of the tricritical points in $T-H$, $T-p$ and $H-p$ planes are shown in Figs. 9 (a),(b) and (c) respectively. The wing lines can be extrapolated to a quantum-tri-critical-point (QTCP) at 0 K, which is found to be at 2.8 T at 5.4 GPa. The shape of the wings at low temperatures was first reported in Ref. 60, based on the third law of thermodynamics and the Clapeyron-Clausius relations. It was pointed out that wings are perpendicular to the $T=0$ K, plane but not perpendicular to the p-axis [60]. Later on, theoretical analysis based on Landau expansion shows that the slope of the wings $\mathrm{d}T/\mathrm{d}H$ and $\mathrm{d}p/\mathrm{d}H$ are infinite near $H=0$ T [61]. This was observed experimentally in URhGe [62]. It was also observed in $LaCrGe_3$, despite the existence of another magnetic phase [14]. Here, we do not observe such behavior $(\mathrm{d}T/\mathrm{d}H|_{TCP}\rightarrow\infty)$ in wings near TCP which could be due to the existence of the magnetic phase MP1 or to

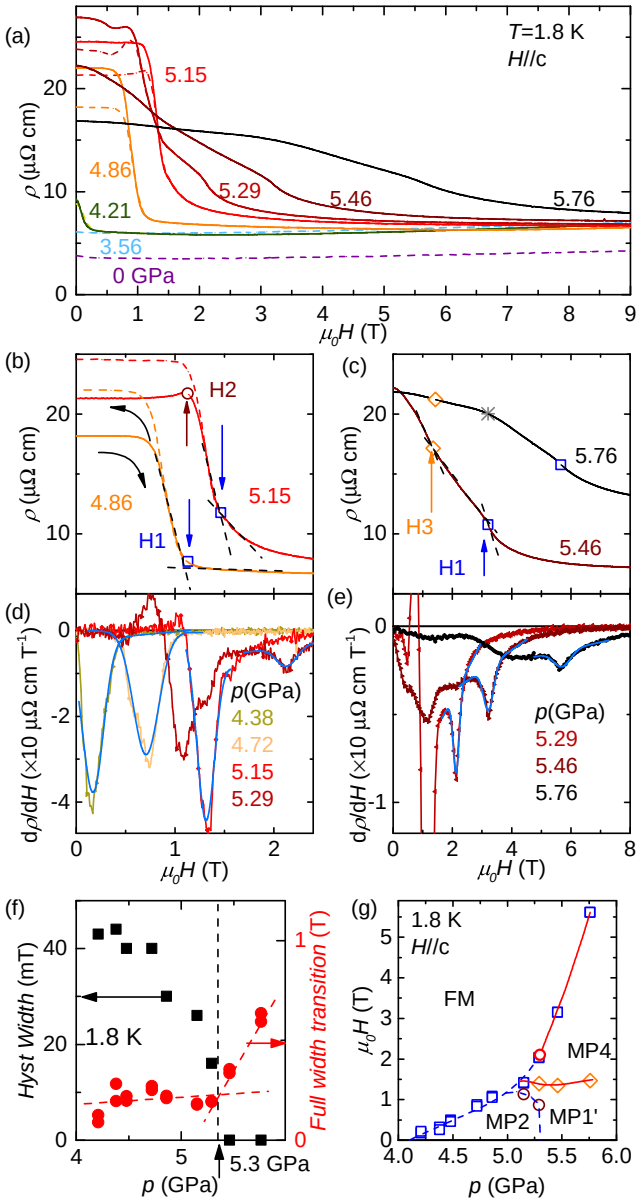

FIG. 8. (Color online) (a) Field dependence of ρ at 1.8 K for various pressures. Continuous and dashed lines represent the field increasing and decreasing respectively. Representative $\rho(H)$ data for (b) 4.1 GPa $< p <$ 5.3 GPa, (c) $p >$ 5.3 GPa and the criteria used to obtain the transition fields at 1.8 K. The open symbols represent the corresponding transition fields. The gray star represents the shoulder like anomaly appeared at 5.76 GPa (Fig. 7). (d)-(e) Representative derivative, dρ/dH data for H1 transition at 1.8 K. The blue color lines represent the Gaussian+linear-background fitted curves which are used to obtained full-width of the H1 transition. (f) left axis shows the pressure dependence hysteresis width of transition H1 at 1.8 K. Right axis shows pressure dependence of the full-width of H1 obtained by dρ/dH ((d)-(e)) at 1.8 K. Vertical dashed line represent the tricritical pressure $\sim$ 5.3 GPa, at 1.8 K. (g) $H - p$ phase diagram at 1.8 K based on the criterion shown in (b,c). Blue and red solid lines represent the first and second order transitions. Red open circle represents the extrapolated QTCP.

the lack of data near p_1. More careful measurements near p_1 are required. Also, the TCP at $H = 0$ T is found to be $\sim$8 K and this is below the MP1 transition. A similar observation was made in $LaCrGe_3$ [14] where the TCP seems to be located below the Lifshitz point. Recent theoretical description by Belitz and Kirkpatrick in Ref. 15 shows the complex behavior of the phase diagrams of metallic magnets when an AFM order is observed in addition to the FM phase due to the quantum fluctuations. Similar to the Fig. 4 (a) in Ref. 15, we observed a QTCP where first order AFM-FM transition changes into the second order AFM-FM transition at 2.8 T at 5.4 GPa (see Fig. 8 (g)). Very recently QTCP has experimentally observed in $NbFe_2$ [63].

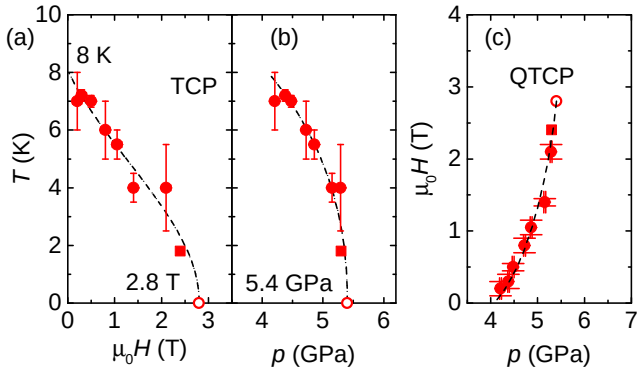

FIG. 9. (Color online) Projection of the tricritical points (TCP) in (a) $T - H$ (b) $T - p$ and (c) $H - p$ planes. Red solid circles represent the TCP determined by Fig. 6(e). Red solid squared obtained from Fig. 8 (f). Dashed lines are guides to the eyes and open red circles represent the extrapolated QTCP.

The constructed, partial, $T - p - H$ phase diagram of $CeTiGe_3$ based on resistivity measurements is shown in Fig. 10. A FM QCP in $CeTiGe_3$ is avoided by the appearance of MP1 and MP2 phases, and shows field induced wing structure above 4.1 GPa. The estimated QTCP is shown by the open red circle. In order to provide clear picture of the wing structure phase diagram, we show only selected phases here (see Fig. 7 for H-T phase diagrams at various pressures). In the case of the itinerant the ferromagnet, $LaCrGe_3$ [12, 14], the second-order FM transition becomes a first order at a tricritical point in the T-p plane and application of a magnetic field reveals a wing structure phase diagram. Appearances of modulated magnetic phase in $LaCrGe_3$ [14] makes it the first example of new type of phase diagram of metallic quantum ferromagnets. Unlike $LaCrGe_3$ (Fig. 5 in Ref. [14]), where, wings are extended beyond the AFM phases, the observed wings in $CeTiGe_3$ are always bounded by the AFM phases. This can be clearly visualized in Fig. 8 (g) (for comparison see Fig. 4 in Ref. [14]). The observation of QTCP in metallic magnets in the case of appearance

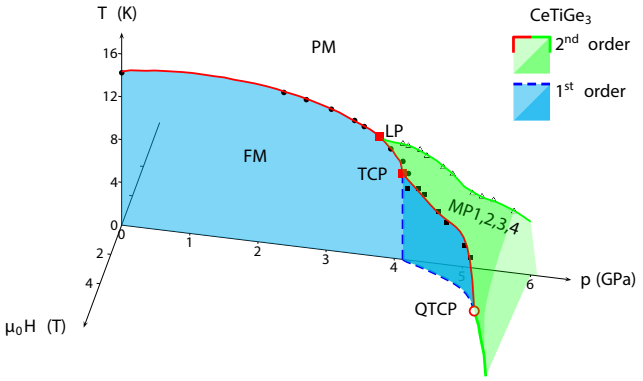

FIG. 10. (Color online) The constructed, partial, $T-p-H$ phase diagram of $CeTiGe_3$ based on resistivity measurements. Blue color surfaces represent the first-order planes and green color surface represents the first-order MP2 phase boundary. Continuous red and blue lines represent the second and first order transition respectively. The open circle represent extrapolated QTCP.

of AFM order in addition to the FM order is theoretically described by Belitz and Kirkpatrick [15]. This theoretical finding is consistent with our experimental observation of QTCP in $CeTiGe_3$. Therefore, $CeTiGe_3$ is a good example of a Ce-based compounds in which the system can be driven into various magnetic ground state by fine tuning of the exchange interaction achieved by temperature, pressure and magnetic field.

CONCLUSIONS

We have measured the high pressure electrical resistivity of $CeTiGe_3$ up to 5.8 GPa and 9 T and found a complex $T-p-H$ phase diagram. The ferromagnetic transition at ambient pressure initially slightly increases and then decreases, indicates that $CeTiGe_3$ is located just below the maximum (left side) of the Doniach phase diagram. The ferromagnetic transition suppresses near 4.1 GPa and cascade of phase transitions are observed above that. Change in residual resistivity near 4.1 GPa and 5.3 GPa suggests a modification of the electronic structure upon entering these magnetic phases. Thus, $CeTiGe_3$ is another clear example of avoided ferromagnetic quantum critical point due to appearance of magnetic phase (probably antiferromagnetic). Application of magnetic field under pressure above 4.1 GPa reveals wing structure phase diagram. In contrast to the wing critical point in $LaCrGe_3$, we observed a tricritical point in H-p plane, which corresponding to the boundary of the wing structure. Estimated quantum tricritical point of $CeTiGe_3$ is located at 2.8 T at 5.4 GPa. We believe that the present work will stimulate further experiments to investigate the properties of this material.

ACKNOWLEDGMENTS

We would like to thank T. Kong, S. Manni and A. Kreyssig for useful discussions. This work was supported by the U.S. Department of Energy (DOE), Office of Science, Basic Energy Sciences, Materials Science and Engineering Division. The research was performed at the Ames Laboratory, which is operated for the U.S. DOE by Iowa State University under contract No. DE-AC02-07CH11358. V.T. was partially supported by Critical Material Institute, an Energy Innovation Hub funded by U.S. DOE, Office of Energy Efficiency and Renewal Energy, Advanced Manufacturing Office.

∗ Current affiliation: Department of Physics, University of California, Davis, California 95616, USA.

[1] M. Brando, D. Belitz, F. M. Grosche, and T. R. Kirkpatrick, Rev. Mod. Phys. **88**, 025006 (2015).
[2] D. Belitz, T. R. Kirkpatrick, and T. Vojta, Phys. Rev. B **55**, 9452 (1997).
[3] D. Belitz, T. R. Kirkpatrick, and T. Vojta, Phys. Rev. Lett. **82**, 4707 (1999).
[4] D. Belitz, T. R. Kirkpatrick, and J. Rollbühler, Phys. Rev. Lett. **94**, 247205 (2005).
[5] V. Taufour, D. Aoki, G. Knebel, and J. Flouquet, Phys. Rev. Lett. **105**, 217201 (2010).
[6] N. Kabeya, H. Maekawa, K. Deguchi, N. Kimura, H. Aoki, and N. K. Sato, J. Phys. Soc. Jpn. **81**, 073706 (2012).
[7] A. V. Chubukov, C. Pépin, and J. Rech, Phys. Rev. Lett. **92**, 147003 (2004).
[8] G. J. Conduit, A. G. Green, and B. D. Simons, Phys. Rev. Lett. **103**, 207201 (2009).
[9] U. Karahasanovic, F. Krüger, and A. G. Green, Phys. Rev. B **85**, 165111 (2012).
[10] S. J. Thomson, F. Krüger, and A. G. Green, Phys. Rev. B **87**, 224203 (2013).
[11] C. J. Pedder, F. Krüger, and A. G. Green, Phys. Rev. B **88**, 165109 (2013).
[12] V. Taufour, U. S. Kaluarachchi, R. Khasanov, M. C. Nguyen, Z. Guguchia, P. K. Biswas, P. Bonfà, R. De Renzi, X. Lin, S. K. Kim, E. D. Mun, H. Kim, Y. Furukawa, C.-Z. Wang, K.-M. Ho, S. L. Bud'ko, and P. C. Canfield, Phys. Rev. Lett. **117**, 037207 (2016).
[13] H. Kotegawa, T. Toyama, S. Kitagawa, H. Tou, R. Yamauchi, E. Matsuoka, and H. Sugawara, J. Phys. Soc. Jpn. **82**, 123711 (2013).
[14] U. S. Kaluarachchi, S. L. Bud'ko, P. C. Canfield, and V. Taufour, Nat. Commun. **8**, 546 (2017).
[15] D. Belitz and T. R. Kirkpatrick, arXiv:1708.00103 (2017).
[16] F. Grosche, S. Julian, N. Mathur, and G. Lonzarich, Physica B **223**, 50 (1996).
[17] N. D. Mathur, F. M. Grosche, S. R. Julian, I. R. Walker, D. M. Freye, R. K. W. Haselwimmer, and G. G. Lonzarich, Nature **394**, 39 (1998).
[18] M. F. Hundley, P. C. Canfield, J. D. Thompson, Z. Fisk, and J. M. Lawrence, Phys. Rev. B **42**, 6842 (1990).
[19] J. R. Iglesias, C. Lacroix, and B. Coqblin, Phys. Rev. B **56**, 11820 (1997).
[20] S. Evans, A. Bhattacharjee, and B. Coqblin, Physica B **171**, 293 (1991).
[21] K. Myers, S. Bud'ko, I. Fisher, Z. Islam, H. Kleinke, A. Lacerda, and P. Canfield, J. Magn. Magn. Mater **205**, 27 (1999).
[22] V. A. Sidorov, E. D. Bauer, N. A. Frederick, J. R. Jeffries, S. Nakatsuji, N. O. Moreno, J. D. Thompson, M. B. Maple, and Z. Fisk, Phys. Rev. B **67**, 224419 (2003).
[23] V. A. Sidorov, E. D. Bauer, H. Lee, S. Nakatsuji, J. D. Thompson, and Z. Fisk, Phys. Rev. B **71**, 094422 (2005).
[24] T. Burghardt, E. Hallmann, and A. Eichler, Physica B **230**, 214 (1997).
[25] A. Yamada, K. Matsubayashi, Y. Uwatoko, K. Kondo, S. Katano, and M. Kosaka, Solid State Commun. **150**, 725 (2010).
[26] M. Inamdar, A. Thamizhavel, and S. K. Dhar, J. Phys. Condens. Matter **26**, 326003 (2014).
[27] P. Manfrinetti, S. Dhar, R. Kulkarni, and A. Morozkin, Solid State Commun. **135**, 444 (2005).
[28] W. Kittler, V. Fritsch, F. Weber, G. Fischer, D. Lamago, G. André, and H. v. Löhneysen, Phys. Rev. B **88**, 165123 (2013).
[29] P. C. Canfield and Z. Fisk, Philos. Mag. B **65**, 1117 (1992).
[30] P. C. Canfield and I. R. Fisher, J. Cryst. Growth **225**, 155 (2001).
[31] P. C. Canfield, T. Kong, U. S. Kaluarachchi, and N. H. Jo, Philos. Mag. **96**, 84 (2016).
[32] E. Colombier and D. Braithwaite, Rev. Sci. Instrum. **78**, 093903 (2007).
[33] N. Tateiwa and Y. Haga, Rev. Sci. Instrum. **80**, 123901 (2009).
[34] G. J. Piermarini, S. Block, and J. Barnett, J. Appl. Phys. **44**, 5377 (1973).
[35] S. Klotz, J.-C. Chervin, P. Munsch, and G. L. Marchand, J. Phys. D: Appl. Phys. **42**, 075413 (2009).
[36] S. K. Kim, M. S. Torikachvili, E. Colombier, A. Thaler, S. L. Bud'ko, and P. C. Canfield, Phys. Rev. B **84**, 134525 (2011).
[37] M. S. Torikachvili, S. K. Kim, E. Colombier, S. L. Bud'ko, and P. C. Canfield, Rev. Sci. Instrum. **86**, 123904 (2015).
[38] B. Bireckoven and J. Wittig, J. Phys. E: Sci. Instrum. **21**, 841 (1988).
[39] B. Cornut and B. Coqblin, Phys. Rev. B **5**, 4541 (1972).
[40] K. Hanzawa, K. Yamada, and K. Yosida, J. Magn. Magn. Mater **47**, 357 (1985).
[41] V. Taufour, H. Hodovanets, S. K. Kim, S. L. Bud'ko, and P. C. Canfield, Phys. Rev. B **88**, 195114 (2013).
[42] A. R. Mackintosh, Phys. Rev. Lett. **9**, 90 (1962).
[43] R. M. Hornreich, M. Luban, and S. Shtrikman, Phys. Rev. Lett. **35**, 1678 (1975).
[44] L. Balicas, S. Nakatsuji, H. Lee, P. Schlottmann, T. P. Murphy, and Z. Fisk, Phys. Rev. B **72**, 064422 (2005).
[45] K.-A. Lorenzer, A. M. Strydom, A. Thamizhavel, and S. Paschen, Phys. Status Solidi B **250**, 464 (2013).
[46] L. Zhao, E. A. Yelland, J. A. N. Bruin, I. Sheikin, P. C. Canfield, V. Fritsch, H. Sakai, A. P. Mackenzie, and C. W. Hicks, Phys. Rev. B **93**, 195124 (2016).
[47] A. Maurya, R. Kulkarni, A. Thamizhavel, D. Paudyal, and S. K. Dhar, J. Phys. Soc. Jpn. **85**, 034720 (2016).
[48] R. E. Baumbach, H. Chudo, H. Yasuoka, F. Ronning, E. D. Bauer, and J. D. Thompson, Phys. Rev. B **85**, 094422 (2012).
[49] Y. Matsumoto, M. Sugi, K. Aoki, Y. Shimizu, N. Kimura, T. Komatsubara, H. Aoki, M. Kimata, T. Terashima, and S. Uji, J. Phys. Soc. Jpn. **80**, 074715 (2011).
[50] H. Aoki, N. Kimura, and T. Terashima, J. Phys. Soc. Jpn. **83**, 072001 (2014).
[51] S. Süllow, M. C. Aronson, B. D. Rainford, and P. Haen, Phys. Rev. Lett. **82**, 2963 (1999).
[52] H. Aoki, S. Uji, A. K. Albessard, and Y. Ōnuki, Phys. Rev. Lett. **71**, 2110 (1993).
[53] H. Wilhelm and D. Jaccard, Solid State Commun. **106**, 239 (1998).
[54] P. Haen, H. Bioud, and T. Fukuhara, Physica B: Condensed Matter **259261**, 85 (1999).
[55] D. Aoki, T. Combier, V. Taufour, T. D. Matsuda,

G. Knebel, H. Kotegawa, and J. Flouquet, J. Phys. Soc. Jpn. **80**, 094711 (2011).
[56] N. Kimura, N. Kabeya, H. Aoki, K. Ohyama, M. Maeda, H. Fujii, M. Kogure, T. Asai, T. Komatsubara, T. Yamamura, and I. Satoh, Phys. Rev. B **92**, 035106 (2015).
[57] V. Taufour, U. S. Kaluarachchi, S. L. Bud'ko, and P. C. Canfield, Physica B (2017), 10.1016/j.physb.2017.08.065.
[58] N. Kimura, M. Endo, T. Isshiki, S. Minagawa, A. Ochiai, H. Aoki, T. Terashima, S. Uji, T. Matsumoto, and G. G. Lonzarich, Phys. Rev. Lett. **92**, 197002 (2004).
[59] M. Uhlarz, C. Pfleiderer, and S. M. Hayden, Phys. Rev. Lett. **93**, 256404 (2004).
[60] T. R. Kirkpatrick and D. Belitz, Phys. Rev. Lett. **115**, 020402 (2015).
[61] V. Taufour, U. S. Kaluarachchi, and V. G. Kogan, Phys. Rev. B **94**, 060410 (2016).
[62] S. Nakamura, T. Sakakibara, Y. Shimizu, S. Kittaka, Y. Kono, Y. Haga, J. Pospísil, and E. Yamamoto, Phys. Rev. B **96**, 094411 (2017).
[63] S. Friedemann, W. J. Duncan, M. Hirschberger, T. W. Bauer, R. Kuchler, A. Neubauer, M. Brando, C. Pfleiderer, and F. M. Grosche, Nat Phys **advance online publication** (2017).